EPJ B
Condensed Matter and Complex Systems
www.epj.org

Eur. Phys. J. B **69**, 65–70 (2009) DOI: 10.1140/epjb/e2009-00114-7

Stochastic resonance and energy optimization in spatially extended dynamical systems

Y.-C. Lai, K. Park and L. Rajagopalan

EDP SCIENCES
Società Italiana di Fisica
Springer

Eur. Phys. J. B **69**, 65–70 (2009)
DOI: 10.1140/epjb/e2009-00114-7

THE EUROPEAN PHYSICAL JOURNAL B

Regular Article

Stochastic resonance and energy optimization in spatially extended dynamical systems

Y.-C. Lai[1,2,a], K. Park[1], and L. Rajagopalan[1]

[1] Department of Electrical Engineering, Arizona State University, Tempe, Arizona 85287, USA
[2] Department of Physics, Arizona State University, Tempe, Arizona 85287, USA

Received 25 November 2008 / Received in final form 19 January 2009
Published online 25 March 2009 –

Abstract. We investigate a class of nonlinear wave equations subject to periodic forcing and noise, and address the issue of energy optimization. Numerically, we use a pseudo-spectral method to solve the nonlinear stochastic partial differential equation and compute the energy of the system as a function of the driving amplitude in the presence of noise. In the fairly general setting where the system possesses two coexisting states, one with low and another with high energy, noise can induce intermittent switchings between the two states. A striking finding is that, for fixed noise, the system energy can be optimized by the driving in a form of resonance. The phenomenon can be explained by the Langevin dynamics of particle motion in a double-well potential system with symmetry breaking. The finding can have applications to small-size devices such as microelectromechanical resonators and to waves in fluid and plasma.

PACS. 05.45.Jn High-dimensional chaos – 05.45.-a Nonlinear dynamics and chaos – 05.40.-a Fluctuation phenomena, random processes, noise, and Brownian motion

1 Introduction

The interplay between noise and deterministic nonlinear dynamics often leads to interesting phenomena, such as noise-induced chaos [1–3], stochastic resonance (SR) [4–6] and coherence resonance [7–9]. For example, when a dynamical system is in a periodic window so as to permit two coexisting invariant sets, one a periodic attractor and another a non-attracting chaotic set, noise can connect the two sets dynamically, leading to a chaotic attractor (noise-induced chaos). In SR, noise can enhance and maximize, often significantly, the response of a nonlinear system to weak signals. In a coherence resonance, noise can induce and optimize the temporal regularity of the system dynamics, regardless of the presence of any external signal. In each of these examples, the particular phenomenon of interest occurs as a result of noise variation. There can conceivably be situations where the "environment" is fixed for all relevant time scales of the system dynamics, but some parameters of the system can be varied in a controllable manner. For instance, a change in the frequency of the driving to a nonlinear system can lead to optimization of the system performance [10–13].

In this paper, we investigate spatially extended nonlinear dynamical systems under external driving, whose amplitude can be controllably changed. In the purely deterministic case, variations of the parameter in a reasonable range cause little change to the system dynamics and in the associated quantities of physical interest. However, drastic changes of these quantities are possible when a small amount of noise is present. For instance, for a nonlinear wave under periodic forcing, without noise, variations of the forcing amplitude may not lead to significant change in the energy of the wave system. The presence of spatially uniform or nonuniform noise can enhance and optimize the system energy via a suitable change in the forcing amplitude. This finding may have practical implications. For example, in small-scale devices such as microlectromechanical resonators [14–17] where a large energy output is often desired, deliberate supply of a small amount of noise can be advantageous. In contrast, in a large-scale wave system, the presence of small random perturbations, even of fixed magnitude, can produce large output energy when an external driving of appropriate amplitude is present, which may cause damages to the surroundings.

In Section 2, we demonstrate the phenomenon of noise-activated energy enhancement and optimization in a class of forced nonlinear wave systems, and justify the reliability of the numerical method that we use to integrate the nonlinear stochastic partial differential equation. In Section 3, we construct a toy model based on symmetry-broken

[a] e-mail: yclai@chaosl.la.asu.edu

potential wells to understand the dynamical mechanism of the phenomenon. Conclusions are offered in Section 4.

2 Noise-activated energy enhancement and optimization

We consider a class of spatially extended dynamical systems described by the following nonlinear partial differential equation (PDE) under periodic forcing and noise:

$$\frac{\partial\phi}{\partial t}+a\frac{\partial^3\phi}{\partial t\partial^2 y}+c\frac{\partial\phi}{\partial y}+f\phi\frac{\partial\phi}{\partial y}+\gamma\phi=-\epsilon\sin(Ky-\Omega t)+D\xi(t), \tag{1}$$

where the parameters a, c, f, and γ represent dispersion, drift, nonlinearity, and dissipation, respectively. The amplitude and the frequency of the forcing are ϵ and Ω, respectively, K represents the wavenumber, D is the noise amplitude, and $\xi(t)$ is a Gaussian process of zero mean and unit variance. Because the forcing is periodic in space, the boundary condition is chosen to be periodic. Equation (1) has been used in fluid mechanics to model regularized long waves [18,19] and in plasma physics for understanding drift waves [20]. To solve equation (1) numerically, we use the pseudospectral method or the collocation method [21,22]. In particular, we discretize the space into N equally spaced grid points, $y_j = j2\pi/N$ for $j = 0, 1, ..., N-1$. To evaluate the spatial derivative terms, the solution is expanded in terms of Fourier series,

$$\phi(y,t)=\sum_{k=-N/2}^{N/2-1}\tilde{\phi}_k(t)e^{iky}.$$

The spectral products $ik\tilde{\phi}_k$ and $(ik)^2\tilde{\phi}_k$ are then formed and transformed into the spatial domain using the inverse FFT to yield $\partial\phi/\partial y$ and $\partial^2\phi/\partial y^2$, respectively. The nonlinear term is evaluated by letting $U_j = \phi(y_j)$ and $V_j = \partial\phi/\partial y$ and evaluating $W_j = V_jU_j$. The Fourier transform of W_j can be shown to be

$$\tilde{w}_k=\sum_{p+q=k}\tilde{u}_p\tilde{v}_q+\sum_{p+q=k\pm N}\tilde{u}_p\tilde{v}_q,$$

where the second term on the right-hand side is the aliasing error that can be removed by disregarding the Fourier co-efficients for which $|k| \geq (1/3)N$ (the 2/3-rule or the truncation rule [21,23]). Time integration is carried out by using the standard second-order Huen's method for numerically solving stochastic differential equations [24].

The initial wave form, or the initial condition, required for solving equation (1) can be conveniently chosen to be one of its steady (solitary) wave solutions in the noiseless case [20]. For $D = 0$, a typical solitary solution is [19,20]

$$\phi(y,t=0)=\phi_a+(\phi_b-\phi_a)\mathrm{sn}^2(c_sy,\kappa), \tag{2}$$

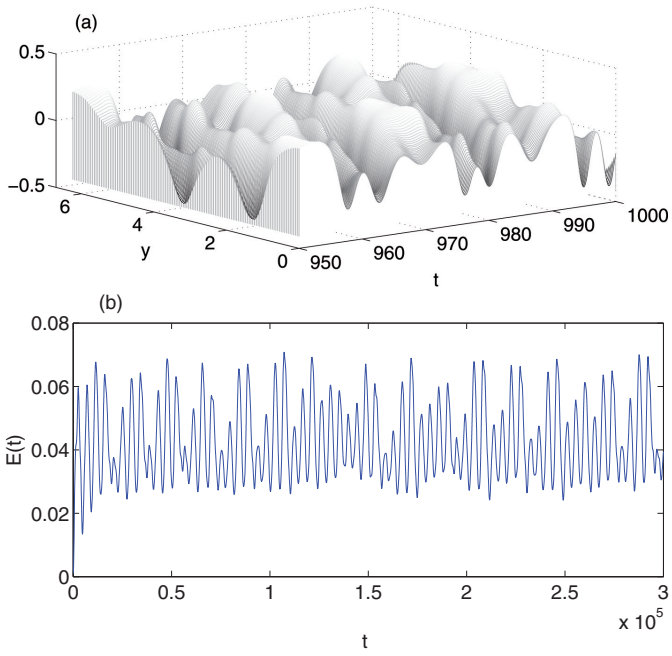

Fig. 1. (Color online) For $D = 0$, $\epsilon = 0.12$, and $\Omega = 0.35$, (a) space-time evolution of a typical wave solution $\phi(y,t)$ of equation (1) and (b) the corresponding energy evolution.

where sn is the Jacobian elliptical function [25], with parameters given by

$$c_s=\sqrt{f(\phi_c-\phi_a)/(12ua)},$$
$$u=c+f(\phi_a+\phi_b+\phi_c)/3,$$
$$\kappa=\sqrt{(\phi_b-\phi_a)/(\phi_c-\phi_a)}.$$

In our computation we fix the following parameter values: $c = 1.0$, $f = -6.0$, $\gamma = 0.1$, $K = 1.0$, $\phi_a = 0$, $\phi_b = 0.0625$, and $\phi_c = 0.125$, which are chosen because the wave system can potentially exhibit distinct energy states [20]. The spatial discretization parameter is chosen to be $N = 128$. The 2π spatial periodicity in the initial solitary wave stipulates the following choice for a: $a = -0.2871$. The forcing amplitude ϵ is taken to be the control parameter. For different choices of the parameters ϵ and Ω, various wave patterns including periodic and turbulent patterns can be generated [20]. A typical solution of equation (1) in the deterministic case ($D = 0$) is shown in Figure 1a, which apparently exhibits features of spatiotemporal chaos.

The wave energy is given by

$$E(t)=\frac{1}{2\pi}\int_0^{2\pi}\left[\phi^2(y,t)-a\left(\frac{\partial\phi(y,t)}{\partial y}\right)^2\right]dy. \tag{3}$$

The evolution of the energy for the wave pattern in Figure 1a is shown in Figure 1b. For nonzero D and ϵ greater than a certain value ϵ_c, the system exhibits two distinct energy states so that the wave energy changes intermittently, as shown in Figure 2. The times that the system stays in the low-energy and high-energy states are found

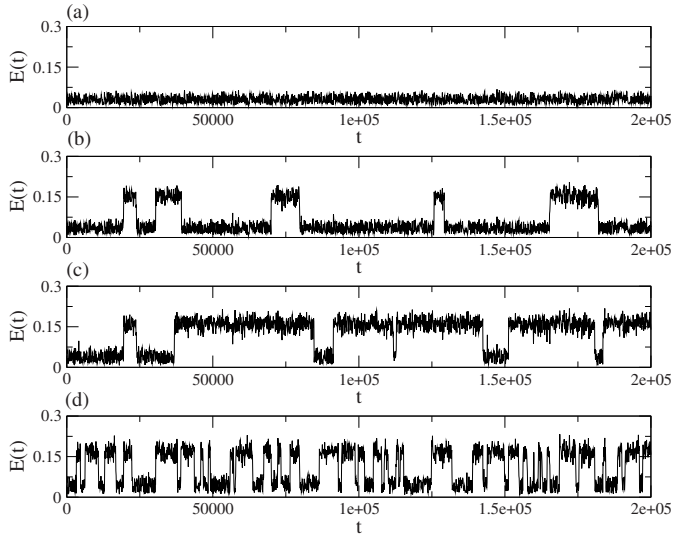

Fig. 2. (Color online) For $D = 0.055$ and $\Omega = 0.65$, evolution of the wave energy for four values of the noise amplitude (a) $\epsilon = 0.11$, (b) $\epsilon = 0.12$, (c) $\epsilon = 0.13$, and (d) $\epsilon = 0.14$.

to be exponentially distributed, and the respective average times depend on the driving amplitude ε. An observation is that the system tends to stay in the high-energy state for relatively long time for moderate value of ε.

How do we ensure that the intermittent energy bursts are not merely a numerical artifact? This issue is particularly important as computations with nonlinear PDEs usually involve more sophisticated integration and transform procedures than those required for ODEs. As for the integration of any PDE, the key factors determining the accuracy, the reliability, and the feasibility of numerical solutions are the step sizes of spatial and temporal discretization. To place a proper grid for spatial discretization, we note that the wavelength of the periodic forcing defines a natural spatial scale for the system. For the wave patterns generated by the model, we find that their spatial scales are not significantly smaller than the forcing wavelength (2π for $K = 1$ in our examples), as can be seen from Figure 1a. Thus, a resolution corresponding to a hundred grid points in the basic 2π cell suffices for spatial discretization. We use $N = 128$. To determine the time step h for numerical integration, we use the following procedure. We set $D = 0$ and first use the forward Euler method to perform the time integration. This method is accurate and stable when the Courant-Friedrich-Levy condition[1] is fulfilled, which states that, given a spatial discretization, a time step larger than some computable quantity should not be taken or, equivalently, the time step should be small to ensure that information has sufficient time to propagate through the spatial discretization. (The comparison is meaningful, of course, when the PDE is in a dimensionless form.) In our case, the computable quantity is energy. Its minimal value is of the order of 10^{-2}. Our first try is thus $h = 10^{-2}$. For the same parameter setting as in Figure 2a, we find that there are energy bursts initially but the solution typically diverges after a finite amount of time, indicating that the bursts observed are artificial and that the step size should be reduced. We find, for $h = 10^{-3}$, there are no energy bursts and the solutions do not diverge, indicating that this choice of the step size may be proper. The forward Euler method is, however, a first-order method. The observation that its solution diverges for $h = 10^{-2}$ but converges for $h = 10^{-3}$ leads to the speculation that, for a higher-order method, solutions would not diverge for both choices of the step size. Indeed, when the fourth-order Runge-Kutta method is used, the solutions are stable and the energy evolutions are qualitatively the same for both step sizes. Furthermore, there are no energy bursts. These experiments thus suggest that for the chosen parameters, *in the deterministic case there should be no energy bursts* and, the choice of $h = 10^{-3}$ is suitable for both low- and high-order methods. For the stochastic case (i.e., $D > 0$), the standard integration routine is typically of low order. This justifies our choice of $h = 10^{-3}$. The systematic tests and reasoning also suggest that the intermittent energy bursts observed for $D > 0$ in Figures 2b–2d are not numerical artifacts but are a genuine behavior of the system. Insofar as the above heuristic rules for choosing the spatial grid size and the time step for integration are followed, the computational results do not depend on variations in these numerical parameters, as we have observed.

To explore the mechanism responsible for the intermittency in energy, it is necessary to examine the phase-space dynamics. A convenient representation of the phase space is the complex, time-dependent coefficient $\tilde{\phi}_k(t)$ in the pseudo-spectral expansion. Alternatively, we can use the amplitude $A_k(t)$ and the phase $\vartheta_k(t)$ of $\tilde{\phi}_k(t)$. Since the initial condition is a solitary wave, it is convenient to use the reference frame riding with this wave: $z = y - \Omega t$ and $\tau = t$. In this frame, the solitary wave is simply a fixed point in the two-dimensional plane $[A_k(\tau), \theta_k(\tau)]$ with a fixed energy, where $\theta_k(\tau) = \vartheta_k(t) + k\Omega t$. This is true for any other planes, say $[A_k(\tau), A_{k+1}(\tau)]$. In the deterministic case ($D = 0$), a wave that generates regular energy oscillations is represented by a cycle in such a plane. as shown in Figure 3a for $D = 0$. As noise is turned on, we expect the cycle to be smeared out and, in addition, the trajectory can wander out of the original region confined by the cycle, generating energy bursts. Such a behavior is shown in Figures 3b and 3c. The intermittent nature of the energy bursts is hinted by the noticeable difference between the densities of the trajectory points in the original, cycle-confined region and in the newly accessible region. Thus we see that, in an infinite dimensional nonlinear system, intermittent energy bursts are generated by a "metamorphic" expansion of the dynamical invariant set in the phase space on which trajectories of the system live. In low-dimensional dynamical systems, this mechanism typically leads to an exponential distribution of the time intervals between successive bursts [26], which also holds for our system, as we have verified numerically.

[1] E.W. Weisstei, "Courant-Friedrich-Levy Condition", From *MathWorld – A Wolfram Web Resource* (`http://mathworld.wolfram.com/Courant-Friedrich-LevyCondition.html`).

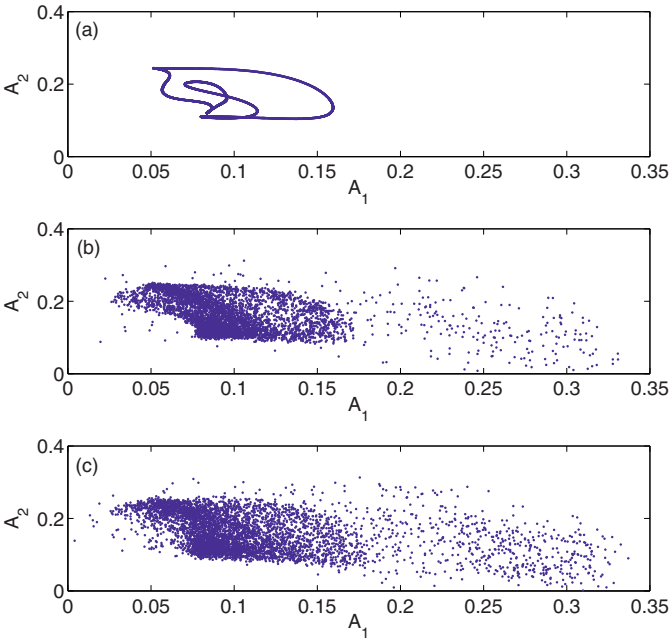

Fig. 3. (Color online) For $\epsilon = 0.193$ and $\Omega = 0.65$, a continuous trajectory in a two-dimensional representation of the phase space: (a) the deterministic case $D = 0$, (b) $D = 0.075$, and (c) $D = 0.125$. For $D = 0$, the dynamical invariant set on which the trajectories live is topologically a cycle, giving rise to regular energy oscillations (Fig. 2a). For $D > 0$, the set explodes to a larger phase-space region, generating intermittent energy bursts (Figs. 2b, 2c).

Regarding the region of the original cycle as the low-energy state and the region that the trajectory bursts into as the high-energy state, we see that, under noise, the system visits the states intermittently. For small forcing amplitude ε, the system tends to spend more time in the low energy state (Fig. 2b), so the average energy of the system is small. For moderate values of ε, the system is more likely to be found in the high-energy state (Fig. 2c), leading to a large average energy. For both cases (Figs. 2b and 2c), the rate at which the system switches between the two states is relatively small. For large values of ε, however, the switching rate is substantially increased, as shown in Figure 2d, which effectively reduces the average energy of the system. All these lead to a "resonance-like" behavior in the system energy as a function of the forcing amplitude, as shown in Figure 4a.

The energy resonance phenomenon can be explained by examining the system's average dwelling times τ_l and τ_h in the low- and high-energy state, respectively. In particular, we find that, as ε is increased, τ_l decreases continuously, so that the probability for the system to stay in the low-energy state keeps decreasing. However, τ_h increases first, reaches a maximum, and then decreases. These behaviors are shown in Figure 4b. The consequence of the combined effect of the behaviors of τ_l and τ_h is that, the average energy of the system increases first, reaches a maximum, and then decreases, leading to the observed resonance-like phenomenon. These observations suggest

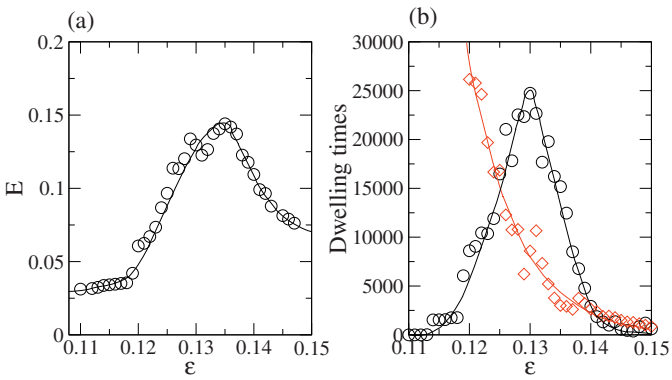

Fig. 4. (Color online) For $D = 0.055$, $\Omega = 0.65$, (a) average wave energy versus the forcing amplitude ε, and (b) average dwelling times of the system in the low (open diamonds) and high (open circles) energy state versus ε.

that, despite the sophisticated spatiotemporal nature of the wave system, the root of the energy resonance phenomenon[2] is likely to have a low-dimensional origin: continuous symmetry breaking in the Langevin dynamics of particle motion in a one-dimensional double potential well system.

3 Toy potential model

Imagine particle motion in a double-well potential system, where noise is present and damping is heavy so that the acceleration of the particle can be neglected. The motion is thus described by the classical Langevin equation, a paradigmatic model for understanding SR [4,5]. In most previous works on SR, the potential wells are chosen to be symmetric and the focus has been on the rate of transitions between the wells. This treatment has indeed proven to be effective when considering measures that depend mainly on the transition rate, such as the signal-to-noise ratio, correlation, entropy [4,5] or even the more recent average phase-synchronization time [27]. The relative times that the particle spends in different wells have no direct influence on these measures, which justifies the symmetry between the wells. Our interest here is in physical quantities that not only depend on the transition rate, but more importantly, assume distinct values when the particle is in different wells. Thus the relative dwelling times of the particle in the wells become the key to our problem.

To break the symmetry in the dwelling time, a convenient approach is to assume that the depths of the wells are different. As a system parameter, say ε, is changed, the depths vary and, in general, their dependences on the parameter will be different. To be concrete, we consider a physical quantity Z of interest that assumes a larger value when the particle is in one of the wells, say the right well. As the depth of the right well is increased, for fixed noise amplitude, the average dwelling time of the particle in the

[2] Similar behaviors have been found for spatially nonuniform noise.

right well will increase. If, at the same time, the depth of the left well is reduced, the particle tends to spend less time in the left well. As a result, $\langle Z \rangle$, the average value of Z, is increased. This trend continues insofar as the right-well depth keeps increasing and simultaneously, the left-well depth decreases. For some optimal value of $\varepsilon = \bar{\varepsilon}$, the right-well depth reaches a maximum. If the left-well depth has become small and does not change appreciably about $\bar{\varepsilon}$, the particle will spend a maximally possible time in the right well, leading to optimization of $\langle Z \rangle$.

A suitable potential system can indeed be constructed based on the above considerations. For instance, we have found the following potential:

$$U(x) = -x^2/2 + x^4/4 + hx + f_1(x,\varepsilon) + f_2(x,\varepsilon), \quad (4)$$

in equation (4), ε is a control parameter, and the functions $f_1(x,\varepsilon)$ and $f_2(x,\varepsilon)$ are given by

$$f_1(x,\varepsilon) = \exp\{a[b - (c - g_1(x,\varepsilon))^2]\},$$
$$f_2(x,\varepsilon) = \exp[dg_2(x)] - 1,$$

where $g_1(x,\varepsilon) = \varepsilon e^{k_1(x-1)}$, $g_2(x,\varepsilon) = \varepsilon e^{K_2(x+1)}$, a, b, c, d, h, k_1, and k_2 are parameters. In the absence of $f_1(x,\varepsilon)$ and $f_2(x,\varepsilon)$, $U(x)$ is a tilted double-well potential with two local minima: one at $x = -1$ and another at $x = +1$. The functions $f_1(x,\varepsilon)$ and $f_2(x,\varepsilon)$ are chosen such that they are appreciable for x near -1 and $+1$, respectively, and they approach zero rapidly as x deviates from their respective local minima. Thus the dependence of the depth of the right-side well on ε is mainly determined by $f_1(+1,\varepsilon)$, and $f_2(-1,\varepsilon)$ determines the dependence of the left-well depth on ε. In particular, as shown in Figure 5a, for $x = +1$, as ε is increased from zero, $f_1(+1,\varepsilon)$ increases, reaches a maximum, and then decreases. However, $f_2(-1,\varepsilon)$ decreases continuously with ε. As a result, the depth of the right well exhibits a pronounced maximum as a function of ε and, in the same ε-range the depth of the left well decreases mostly and attains a local miminum for a value of ε near that for which the right well depth reaches maximum. These features are precisely what is required for the symmetry-breaking phenomenon described in the preceding paragraph.

An example of the dependences of the depths of the potential wells on the control parameter ε is shown in Figure 5a. Theoretically, the average dwelling time of a particle in a well is given by the Kramer's formula [28]. To obtain the actual dwelling times, we simulate the Langevin dynamics:

$$dx/dt = -dU/dx + D\xi(t),$$

where $\xi(t)$ is a Gaussian random process of zero mean and unit variance. The resulting dwelling times T_l (open squares) and T_r (open circles) in the left and right well, respectively, are shown in Figure 5b as functions of ε for $D = 0.28$. We observe that T_r exhibits a pronounced maximum for $\bar{\varepsilon} \approx 2$, about which T_l assumes much smaller values. Suppose the physical quantity Z possesses larger values when the particle is in the right well. We can then expect Z to be maximized about $\bar{\varepsilon}$.

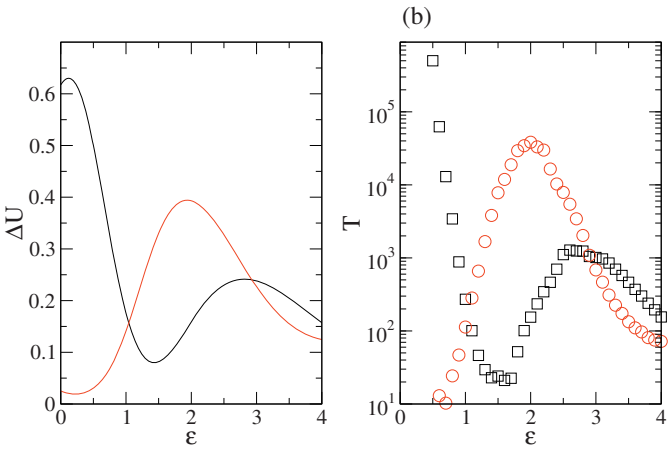

Fig. 5. (Color online) For the potential system (4), (a) the depths of the right (red) and the left (black) potential wells versus the control parameter ε, and (b) the actual dwelling time of a Langevin particle in the right (red, open circles) and in the left (black, open squares) wells. Parameters are $a = 0.3$, $b = 0.56$, $c = 0.6$, $d = 0.13$, $e = -0.35$, $f = -1$, and $g = 0.3$.

4 Conclusion

In summary, we have uncovered a phenomenon in spatiotemporal dynamical systems described by nonlinear PDEs: in a noisy environment, physical quantities such as the wave energy can be optimized by continuous variation of a control parameter. The dynamical mechanism for this phenomenon contains two essential ingredients: (1) noise-induced switchings between two coexisting states with distinct values of energy and (2) symmetry breaking in the dwelling times of the system in the two states. Langevin dynamics in a class of asymmetric double-well potential provides a physically intuitive understanding of these ingredients. The energy optimization problem in spatially extended dynamical systems can be important for applications such as enhancing energy output in small-scale systems, e.g., microelectromechanical resonators, mathematically also described by nonlinear PDEs. On the contrary, large energy output can be of significant concern in other spatiotemporal systems such as fluid and plasma systems, where abnormally large energy may cause severe damage to the system and surroundings.

This work is supported by AFOSR under Grant No. FA9550-06-1-0024.

References

1. A. Hamm, T. Tél, R. Graham, Phys. Lett. A **185**, 313 (1994)
2. L. Billings, I.B. Schwartz, J. Math. Bio. **44**, 33 (2002)
3. Y.C. Lai, Z. Liu, L. Billings, I.B. Schwartz, Phys. Rev. E **67**, 026210 (2003)

4. K. Wiesenfeld, F. Moss, Nature **373**, 33 (1995)
5. L. Gammaitoni, P. Hänggi, P. Jung, F. Marchesoni, Rev. Mod. Phys. **70**, 223 (1998)
6. P. Hänggi, Chem. Phys. Chem. **3**, 285 (2002)
7. D. Sigeti, W. Horsthemke, J. Stat. Phys. **54**, 1217 (1989)
8. A.S. Pikovsky, J. Kurths, Phys. Rev. Lett. **78**, 775 (1997)
9. Y.C. Lai, Z. Liu, Phys. Rev. Lett. **86**, 4737 (2001)
10. L. Gammaitoni, F. Marchesoni, S. Santucci, Phys. Rev. Lett. **74**, 1052 (1995)
11. S. Barbay, G. Giacomelli, F. Martin, Phys. Rev. E **62**, 157 (2000)
12. S.G. Lee, S. Kim, Phys. Rev. E **72**, 061906 (2005)
13. K. Park, Y.C. Lai, S. Krishnamoorthy, Chaos **17**, 043111 (2007)
14. H.G. Craighead, Science **290**, 1532 (2000)
15. X.M.H. Huang, C.A. Zorman, M. Mehregany, M.L. Roukes, Nature **321**, 496 (2003)
16. S.K. De, N.R. Aluru, Phys. Rev. Lett. **94**, 204101 (2005)
17. S.B. Shim, M. Imboden, P. Mohanty, Science **316**, 95 (2007)
18. A. Hasegawa, K. Mima, Phys. Fluids **21**, 87 (1978)
19. J.D. Meiss, W. Horton, Phys. Fluids **25**, 1838 (1982)
20. K.F. He, A. Salat, Plasma Phys. Controlled Fus. **31**, 123 (1989)
21. C. Canuto, M.Y. Hussaini, A. Quarteroni, T.A. Zang, *Spectral Methods in Fluid Dynamics* (Springer, Berlin, Germany, 1988)
22. B. Fornberg, *Practical Guide to Pseudospectral Methods* (Cambridge University Press, Cambridge, UK, 1998)
23. S.A. Orszag, Phys. Fluids Supp. II **12**, 250 (1969)
24. P.E. Kloden, E. Platen, *Numerical Solution of Stochastic Differential Equations* (Springer, Berlin, Germany, 1992)
25. P.F. Byrd, M.D. Friedman, *Handbook of Elliptic Integrals for Engineers and Scientists* (Springer-Verlag, New York, 1971)
26. D. Marthaler, D. Armbruster, Y.C. Lai, E.J. Kostelich, Phys. Rev. E **64**, 016220 (2001)
27. K. Park, Y.C. Lai, Europhys. Lett. **70**, 432 (2005)
28. P. Hänggi, P. Talkner, M. Borkovec, Rev. Mod. Phys. **62**, 251 (1999)